Journal of Non-Crystalline Solids 431 (2016) 135–139

Contents lists available at ScienceDirect

Journal of Non-Crystalline Solids

journal homepage: www.elsevier.com/ locate/ jnoncrysol

Optical and structural properties of Mn^{2+} doped $PbGeO_3$–$SbPO_4$ glasses and glass–ceramics

V. Volpi [a], M. Montesso [a,b], S.J.L. Ribeiro [b], W.R. Viali [a], C.J. Magon [c], I.D.A. Silva [c], J.P. Donoso [c], M. Nalin [a,b,*]

[a] Chemistry Department, Federal University of São Carlos, São Carlos, SP, Brazil
[b] Chemistry Institute, São Paulo State University, Araraquara, SP, Brazil
[c] Physics Institute, University of São Paulo, São Carlos, SP, Brazil

ARTICLE INFO

Article history:
Received 19 December 2014
Received in revised form 9 April 2015
Accepted 11 April 2015
Available online 17 April 2015

Keywords:
Glass;
Glass–ceramic;
Manganese;
UV–Vis;
EPR

ABSTRACT

This paper shows the study of optical and structural properties of $SbPO_4$–$PbGeO_3$–$MnCl_2$ glass and glass–ceramics. Glass was prepared by melting–quenching methodology while the glass ceramic was obtained by controlled thermal treatment of the glass. The UV–Vis results show that the glass presents only Mn^{2+} species, but, the thermal treatment leads to oxidation of Mn^{2+} to Mn^{3+} species, what was evidenced by an absorption band in the visible range. High resolution transmission electron microscopy shows the presence of nanocrystalline phases of Mn_2O_3 and $PbGeO_3$ confirming the formation of a glass–ceramic. Electron paramagnetic resonance measurements suggest that manganese ions occupy only one environment in the glass. On the other hand, for glass–ceramic at least three different structural sites were identified by simulation of the EPR signal.

1. Introduction

The advantage of glasses over other inorganic materials is the possibility to tune their compositions in order to obtain a suitable matrix where it is possible to dissolve, disperse and stabilize a large variety of ions and nanoparticles. Paramagnetic glasses and glass–ceramics containing transition metal oxides have been studied in the last years due to their interesting luminescent and magneto-optical properties [1–4]. In particular, manganese is one of the most studied species due to its interesting chemical properties, such as, the large variety of oxidation states allowing its uses in several technological fields. Visible luminescence [1,2,5–7], magnetic sensors [8] and magneto-optical recording [3] are among the possible applications of such element embedded in glasses. Optical and magneto-optical properties depend on the environments and valence states of the manganese ions. A large amount of papers are found in the literature regarding both fundamental and application point of views, moreover, many doubts are still in discussion with respect to what oxidation states and in what environments are Mn ions into the glasses and glass–ceramics prepared by thermal treatment of the glasses. Usually, manganese is added into glass matrixes as minor component and for this reason Mn^{2+} ions do not drive to strong colored glasses due to the low absorptivity [9]. On the other hand, more concentrated samples may lead to formation of higher oxidation states (Mn^{3+} or Mn^{4+}) leading to colored glasses [1,9,10].

Electron paramagnetic resonance, EPR, is a sensitive spectroscopic technique for the study of local coordination environment of paramagnetic centers, such as transition-metal and rare-earth ions, incorporated in a variety of materials. In particular, EPR has been extensively used to probe the electronic environment of paramagnetic manganese species. Common valence states of manganese are +2, +3 and +4. The three-fold state, although paramagnetic, is usually not observable by EPR at low frequency due to the large zero field splitting as well as shorter spin relaxation times [11]. Both two and fourfold states can, indeed, be detected even at room temperature. EPR of Mn^{4+} ions ($3d^3$, $S = 3/2$) has been reported in manganese complex [12,13], layered oxides [14] and titanium oxide based systems [15,16]. Mn^{2+} is, by far, the manganese valence mostly studied by EPR in glasses [17–21].

Heavy metal oxide glasses, especially those based on antimony and germanium, are very interesting compositions for optical uses and have been studied due to their good transparency, high polarizability, high thermal expansion, low dispersion, high linear and non-linear refractive index and solubility for rare earths [22–26].

The symbiosis between the magneto-optical effects of manganese ions and the optical properties of heavy metal oxide glasses is interesting for photonic applications. In this sense, in the present study new optical glasses and glass–ceramics were obtained in Mn-containing $PbGeO_3$–$SbPO_4$ system and an extensive investigation on the optical and structural properties was undertaken. The studies were also extended to the valence states and coordination of manganese in the

* Corresponding author at: Chemistry Institute, São Paulo State University, Araraquara, SP, Brazil.
E-mail address: mnalin@iq.unesp.br (M. Nalin).

http://dx.doi.org/10.1016/j.jnoncrysol.2015.04.022
0022-3093/

glass network by different techniques including UV–Vis and Raman spectroscopies, differential scanning calorimetry (DSC), X-ray diffraction, electronic paramagnetic resonance, EPR and high resolution transmission electron microscopy, HRTEM.

2. Experimental procedure

2.1. Glass synthesis

The synthesis of $PbGeO_3$–$SbPO_4$:$MnCl_2$ glass was done in two steps:

Step 1 consisted of the preparation of lead germanate glass, $PbGeO_3$ following the study done earlier by L.A. Bueno [27]. Equimolar amounts of raw materials PbO and of GeO_2 (PbO Synth grade purity 98,0% and GeO_2 Aldrich grade purity 99,0%) were thoroughly mixed in agate mortar and melted in platinum crucible at 950 °C for about 30 min. The resultant melt was casted between two stainless steel plates at room temperature.

In step 2, vitreous $PbGeO_3$ was mixed to $SbPO_4$ and $MnCl_2$ in the following molar ratio 89.1$PbGeO_3$–9.9$SbPO_4$–1$MnCl_2$ ($SbPO_4$ was prepared as described earlier [28] and $MnCl_2$, Synth grade purity 98,0%). The glass composition was named V1. The composition was then mixed in agate mortar and melted in platinum crucible at 1100 °C for 30 min. The melt was casted into a pre-heated stainless steel mold at 380 °C (value obtained from DSC measurements). The glass was left at such temperature during 2 h before to be cooled down to room temperature.

2.2. Glass ceramic preparation

The glass ceramic was prepared by treating the glass above the glass transition temperature. The temperature chosen was 450 °C. The glass piece, measuring 1 cm × 1 cm × 500 μm was heated in an adapted furnace which was introduced into the spectrophotometer allowing to follow the evolution of the treatment, in situ, in the UV–Vis range. The sample obtained after thermal treatment was named V1-GC.

2.3. Glass characterization

The characteristic temperatures of the glasses (Tg for glass transition temperature, Tx for onset of crystallization and Tp for maximum of crystallization peak) were determined by differential scanning calorimetry (DSC). Measurement was carried out using an equipment TA Instruments, model TA 2910. Powdered sample was heated at 10 °C min^{-1} in aluminum pans under N_2 atmosphere in the range from 100 to 600 °C. The estimated errors were 2 °C for Tg and Tx temperatures and 1 °C for Tp. The amorphous structure of the glasses was confirmed by X-ray diffraction using a Siemens Crystalloflex Diffractometer with Cuκα radiation in the range of 2θ from 4 to 70°.

UV–Vis absorption spectra of glasses were obtained "in situ" in the range from 200 to 800 nm using an adapted furnace coupled to a Varian, Cary 5000 scan spectrometer.

X-band CW-EPR spectra were recorded at 15 K on a Bruker Elexsys E580 spectrometer operating at 9.485 GHz, equipped with a continuous flow liquid helium Oxford cryogenic system. Solid state powder EPR spectra were simulated by the well-known software package named EasySpin [29], implemented in MATLAB (MathWorks, Inc.).

Transmission electron microscopy (TEM) was performed to assess the structural information of the passivated nanoparticles. Low-magnification and high-resolution transmission electron microscopy images (HR-TEM) were obtained using the JEOL 3010 TEM-HR operating at 300 kV. Fast Fourier Transforms (FFTs) of TEM images were obtained using the Digital Micrograph (Gatan) software to obtain the lattice d-spacing. For TEM analysis the sample dispersed in isopropyl alcohol was deposited on a copper grid covered with an amorphous carbon film and left to dry in Ar-atmosphere.

3. Results and discussion

Homogenous, transparent pale-yellow glass samples of composition 89.1$PbGeO_3$–9.9$SbPO_4$–1$MnCl_2$ were obtained. Characteristic temperatures could be easily observed in DSC curves, Fig. 1, while the non-crystalline structure was confirmed by X-ray diffraction (inset in Fig. 1). From DSC results it is noticed that the stability parameter (i.e. the difference between the glass transition and onset of crystallization temperatures) is around 94 °C allowing the preparation of bulk samples 3 mm thick. In order to study the effect of the temperature on the optical properties of the glass, a controlled heat treatment was performed as described earlier in the experimental section.

The thermal treatment was monitored "in-situ" by using a UV–Vis spectrophotometer and Fig. 2 shows absorption spectra obtained each 10 min. d–d transitions due to the d^5 configuration of Mn^{2+}, occurring usually in the 300–450 nm for oxide glasses are not observed, probably due to low relative Mn^{2+} content and strong overlap with the host glass band gap [3].

The glass color was observed to change to purple (inset of Fig. 2) and in fact, after 90 min of heat treatment it is possible to observe a rising band around 513 nm (red curve in Fig. 2). The intensity of such band increases while it shifts to lower wavelengths, up to 538 nm (blue curve), observed for 230 min of treatment. Fig. 2 also shows a second absorption band appearing as a shoulder at around 615 nm. For longer heat treatments the broad absorption band is observed to shift to smaller wavelengths, being centered at 525 nm after 400 min (purple curve). The shoulder remains unchanged.

Purple color in Mn doped glasses is usually attributed to the presence of Mn^{3+} ions which in general present higher absorption coefficients than Mn^{2+} [9]. Heat treatments lead to formation of Mn^{3+} species because treatments above the glass transition would allow the diffusion of oxygen through the glass leading to oxidation of divalent to trivalent Mn ions. The shoulder, or asymmetry, around 615 nm has been interpreted as been the result of a Jahn–Teller tetragonal distortion of the octahedral ligand field around MnO_6 units and was observed in silicates, borates and sodium phosphate glasses containing manganese ions [30].

The TEM images of the heat treated sample, Fig. 3, revealed the presence of crystalline nanoparticles, homogeneously dispersed through the glass (Fig. 3a). The particle size histogram for the glass sample, obtained

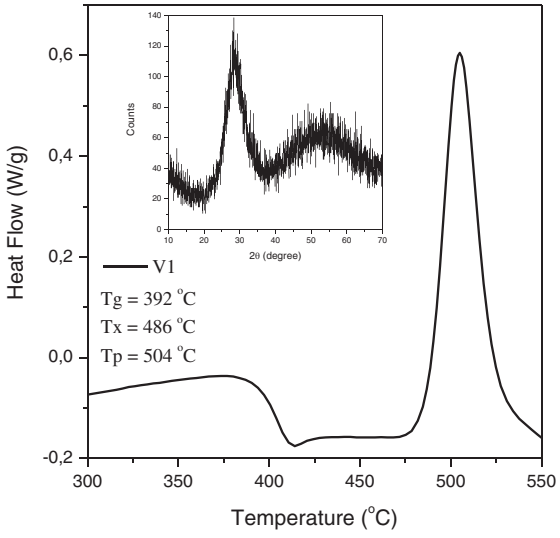

Fig. 1. DSC curve of the antimony–lead germanate glass containing Mn^{2+}. Inset shows the amorphous X-ray diffraction pattern of the same sample.

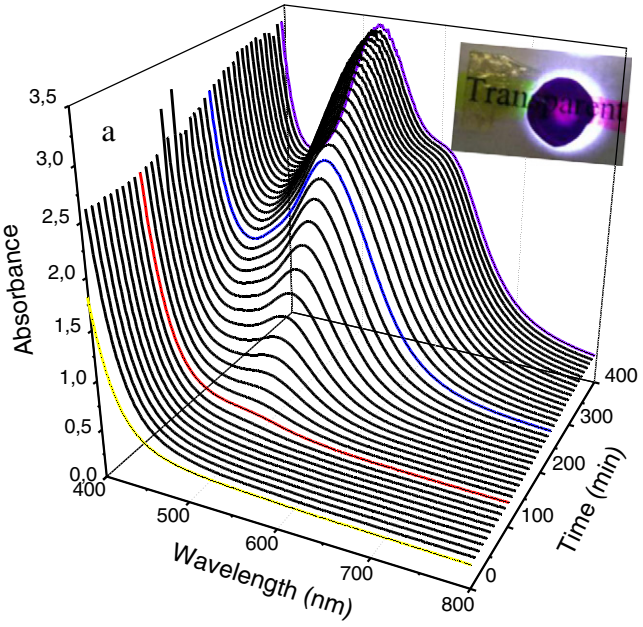

Fig. 2. UV–Vis absorption curves obtained in-situ from the glass doped with manganese. Inset shows the photography of the glass before and after thermal treatment.

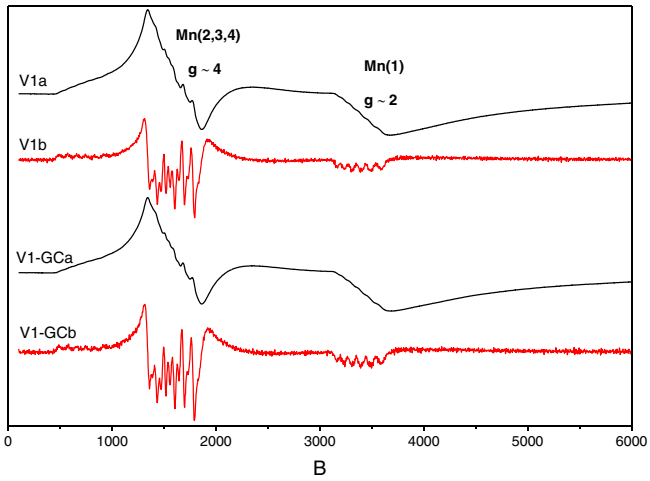

Fig. 4. Experimental EPR spectra of 89.1$PbGeO_3$–9.9$SbPO_4$–$MnCl_2$ of the non-treated glass (V1a) and the glass treated at 450 °C (V1-GCa). In (V1b) and (V1-GCb) are shown the numerical second derivative of both spectra, respectively. Spin Hamiltonian parameters are shown in Table 1. Structured spectra at $g \approx 2$ and $g \approx 4$ are attributed to Mn^{2+} site (1) and site (2,3,4) species, respectively, as explained in the text.

from the TEM micrographs, is shown as an inset, where vertical bars represent the experimental data, while the solid line results from the curve fitting of the data using the log-normal distribution function [31]. Values of the average particle diameter (D_{TEM}) and distribution width standard diameter deviation (w) obtained from the fitting of the data presented in the histogram were 4.9 ± 0.1 nm and 0.2, respectively.

Interplanar distances could be measured in HR-TEM micrographs (Fig. 3b). The shortest, measuring 2.50 Å corresponds to the (110) Bragg plane reflection of bulk rhombohedral Mn_2O_3 (JCPDS Card No. 33-900) and the longest one, measuring 3.28 Å was assigned to the (222) Bragg plane reflection of bulk monoclinic $PbGeO_3$ (JCPDS Card No. 31-684). The inset in Fig. 3b shows the FFT patterns, used to stipulate the interplanar distances. These findings indicate two different crystalline nanoparticles dispersed into the glass ceramic and also confirm the presence of Mn^{3+} ions.

In order to investigate the coordination environment of the manganese ions an EPR investigation was performed. Fig. 4 shows the X-band EPR spectra of Mn^{2+} doped glass sample in the vitreous phase, Fig. 4 (V1a), and after thermal treatment at 450 °C, Fig. 4 (V1-GCa). Two prominent features with effective *g*-values $g \approx 2$ and $g \approx 4$ appeared in the spectra. The former signal, which has been frequently reported in glasses [17,32–34] is attributed to magnetically isolated Mn^{2+} ions in symmetry close to octahedral or undistorted cubic sites. The low field signal at $g \approx 4$ is associated with isolated Mn^{2+} ions in rhombic distorted sites subjected to high crystal field effects [33,35–37]. The Mn^{2+} ion has a $3d^5$ electronic configuration and spin $S = 5/2$. Manganese has a stable isotope with non-zero nuclear spin, ^{55}Mn, with $I = 5/2$ (100% natural abundance). Therefore, the EPR spectrum is expected to show a hyperfine structure composed of six lines, resulting from the dipole–dipole interaction between the magnetic moment of the ^{55}Mn nuclei and the electronic moment of the paramagnetic Mn^{2+} ion. Some overlap between the lines can be observed when their linewidth is comparable to the hyperfine splitting constant, *A*.

For a better view of the Mn hyperfine structures, the second derivative spectra were calculated and are displayed in Fig. 4 (V1b, V1-GCb). It is evident the resolution enhancement obtained by this simple signal processing technique. The partial spectrum centered at $g \approx 2$ is insensitive to the thermal treatment and exhibits a well resolved sextet

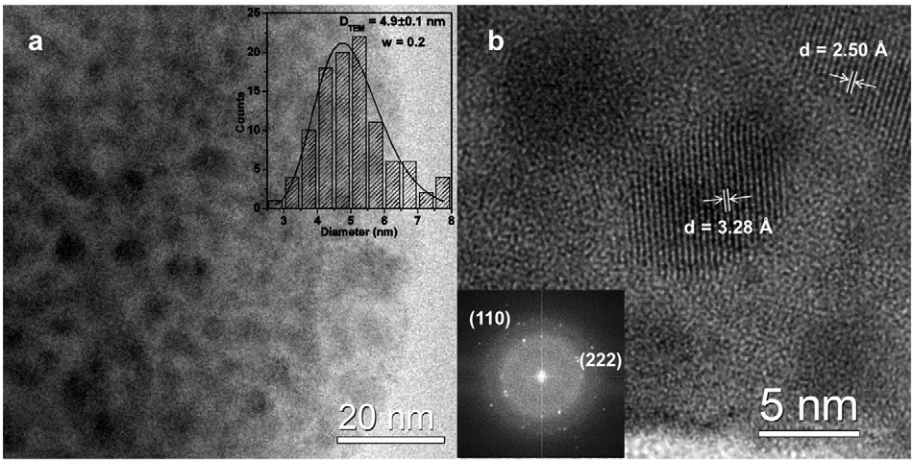

Fig. 3. a) Bright field of the glass–ceramics. Inset shows the histogram of the corresponding image. b) High-resolution TEM images of the nanoparticles. Inset shows the Fast Fourier Transform (FFT) of the corresponding HR-TEM images.

structure superimposed on a broader background. In this case, the hyperfine splitting constant, A, was determined using the procedure given in the literature [36,38] and the result is listed in Table 1, under the denomination of site (1) species.

For most of the reported EPR studies in manganese-doped glasses, the signal at $g \approx 4$ is weak if compared to the main resonance at $g \approx 2$; besides, the hyperfine structure is not resolved at the former signal [17,32–34,39]. For our experimental data, the structure observed at $g \approx 4$ is not weak and is also insensitive to the thermal treatment. Therefore, we simulated the second derivative spectrum of the treated sample shown in Fig. 4 (V1-GCb), at $g \approx 4$, taking into account a Mn ion with isotropic Zeeman and hyperfine interactions. Our conclusion was that the spectrum is too complex to be simulated by only one Mn environment and, indeed, at least three different sites were needed to reproduce the main features of the signal.

The result of the simulation of the $g \approx 4$ structured spectrum of the glass treated sample is displayed in Fig. 5 and the best values for the spin Hamiltonian parameters are listed in Table 1. The line shapes were described by a combination of Gaussian and Lorentzian shapes. A broad spectral component, shown in Fig. 4, was necessary to be included in the simulation. One can notice that the left side of the spectrum, below 1600 G, could be well fitted by a single Mn site, but, for the remaining right side two additional sites were needed. The different Mn environments were numbered by site (2), site (3) and site (4). They are related to magnetically isolated manganese ions. The analysis of the EPR parameters for these sites shows that species (2) and (3) differ from species (4) mainly in the value of the hyperfine constant, which are definitely lower for species (4). The fitting is capable to reproduce well the positions of all lines, although large errors in the amplitudes can be verified. These amplitude errors may result from the fact that the real broadening mechanisms were not well described by the simple line shape assumption and that, a larger number of Mn environments coexist in the glass–ceramic matrix. In general, the hyperfine constants displayed in Table 1, are consistent with those previously reported in the literature for GeO_2 based glasses [25].

The magnitude of the hyperfine constant, A, provides a qualitative measure of the bonding character between the Mn^{2+} ion and its ligands. Van Wieringen determined empirically a correlation between A and the ionicity of the manganese ligand bond and noted that the strength of the hyperfine splitting depends on the glass matrix into which the ion is inserted and is mainly determined by the electronegativity of the neighbors [40,41]. In fluorite crystals, where the bonds are ionic, $A \approx 100 \times 10^{-4}\ cm^{-1}$, while covalent semiconductors like Mn–Te have A values as low as $60 \times 10^{-4}\ cm^{-1}$ [33,42]. The magnitude of the hyperfine splitting value obtained in the present article reveals that the bond between Mn^{2+} ions and the surrounding ligands, $A = (80 - 97) \times 10^{-4}\ cm^{-1}$, is moderately ionic.

The results demonstrate the potential of such glasses to be used as hosts for magnetic nanoparticles since crystalline Mn_2O_3 presents magnetic behavior and may be studied for magneto-optical applications. In this sense, more studies are actually under consideration in our laboratory concerning the increasing of the concentration of Mn into the glass host and the evaluation of the optical and magnetic properties of such new materials.

Table 1
Spin Hamiltonian parameters obtained from numerical simulation of the second derivative spectrum of $89.1PbGeO_3$–$9.9SbPO_4$–$MnCl_2$ glass–ceramic prepared at 450 °C.

Mn species	g (± 0.002)	A ($^{\pm}0.2 * 10^{-4}\ cm^{-1}$)
Mn (1)	2.005	$84.2 \times 10^{-4}\ cm^{-1}$ (232 MHz, 83 G)
Mn (2)	4.640	$94.2 \times 10^{-4}\ cm^{-1}$ (260 MHz, 92.8 G)
Mn (3)	3.932	$97.7 \times 10^{-4}\ cm^{-1}$ (270 MHz, 96.3 G)
Mn (4)	3.960	$80.1 \times 10^{-4}\ cm^{-1}$ (221 MHz, 78.9 G)

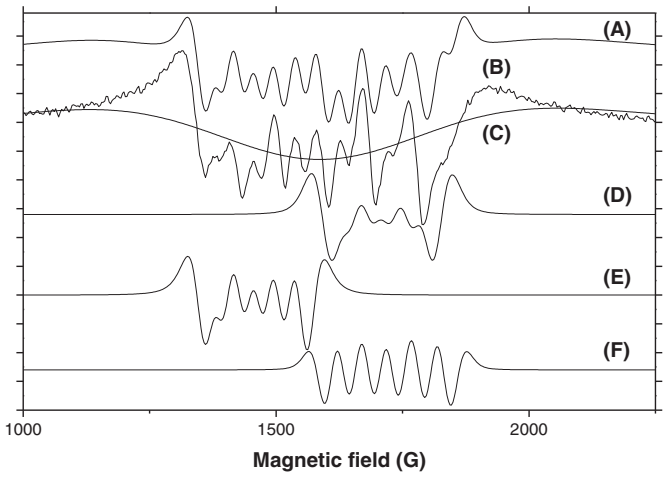

Fig. 5. Second derivative EPR spectrum of $89.1PbGeO_3$–$9.9SbPO_4$–$MnCl_2$ glass treated at 450 °C in the range 1000–2500 G. (A) Simulated spectrum. (B) Experimental spectrum. (C) Broad component: $S = 1/2$, $g = 4.269$. (D) site (4) species. (E) Mn site (2) species. (F) Mn site (3) species. Spin Hamiltonian parameters are shown in Table 1.

4. Conclusions

The influence of the thermal treatment in the glass composition $89.1PbGeO_3$–$9.9SbPO_4$–$MnCl_2$ was studied using several techniques. It was verified that thermal treatment leads to oxidation of Mn^{2+} to Mn^{3+} species and such statement was confirmed by in-situ UV–Vis and HRTEM. TEM images showed two crystalline compounds ascribed to Mn_2O_3 and $PbGeO_3$ phases. The EPR spectrum of the glass was simulated by only one environment, but at least three different sites were needed to reproduce the main features of the EPR signal of the glass–ceramic sample, suggesting a larger number of Mn environments coexist in the glass–ceramic.

Acknowledgments

Financial support of the Brazilian agencies Capes/PNPD grant # 2654/2011 and grant # 2013/07793-6 São Paulo Research Foundation FAPESP/CEPID are gratefully acknowledged. The authors would like to thank LME/LNNano/CNPEM for technical support during electron microscopy investigation.

References

[1] N. Da, M. Peng, S. Krolikowski, L. Wondraczek, Opt. Express 18 (2010) 2549–2557.
[2] A.R. Molla, R.P.S. Chakradhar, C.R. Kesavulu, J.R. Rao, S.K. Biswas, J. Alloys Compd. 512 (2012) 105–114.
[3] A. Winterstein, H. Akamatsu, D. Moncke, K. Tanaka, M.A. Schimidt, L. Wondraczek, Opt. Mater. Express 3 (2013) 184–193.
[4] C. Worsch, M. Buttner, P. Schaaf, R. Harizanova, C. Russel, F. Schimidt, P. Seidel, J. Mater. Sci. 48 (2013) 2299–2307.
[5] L.E. Orgel, J. Chem. Phys. 23 (1955) 1824.
[6] S. Parke, R.S. Webb, Phys. Chem. Glasses 13 (1972) 157.
[7] D. Simkin, K. Oyama-Gannon, P. Menassa, P. Taylor, J. Lumin. 24 (1981) 107.
[8] V.S. Raghuwanshi, R. Harezanova, S. Haas, D. Tatchev, I. Gugov, C. Dewhurst, C. Russel, A. Haell, J. Non-Cryst. Solids 385 (2014) 24–29.
[9] D. Moncke, M. Papageorgou, A. Winterstein-Beckmann, N. Zacharias, J. Archaeol. Sci. 46 (2014) 23–36.
[10] I. Ardelean, M. Peteanu, S. Filip, V. Simon, J. Todor, Solid State Commun. 105 (1998) 339–344.
[11] S.K. Misra, Appl. Magn. Reson. 24 (2003) 127–144.
[12] S. Romain, C. Baffert, C. Duboc, J.C. Leprêtre, A. Deronzier, M.N. Collomb, Inorg. Chem. 48 (2009) 3125–3131.
[13] G. Yin, J.M. McCormick, M. Buchalova, A.M. Danby, K. Rodgers, V.W. Day, K. Smith, C.M. Perkins, D. Kitko, J.D. Carter, W.M. Scheper, D.H. Busch, Inorg. Chem. 45 (2006) 8052–8061.
[14] R. Stoyanovaa, E. Zhechevaa, S. Vassilev, J. Solid State Chem. 179 (2006) 378–388.
[15] S. Güler, B. Rameev, R.I. Khaibullin, O.N. Lopatin, B. Aktas, J. Magn. Magn. Mater. 322 (2010) L13–L17.
[16] A.F.M.Y. Haider, A. Edgar, J. Phys. C 13 (1980) 6239–6250.

[17] J. Kliava, Phys. Status Solidi B 134 (1986) 411–455.
[18] G. Fuxi, L. Huimin, J. Non-Cryst. Solids 95–96 (1987) 61–70.
[19] D.L. Griscom, Electron Spin Resonance, in: D.R. Uhlman, N.J. Kreidl (Eds.), Glass, Science and Technology, vol. 4B, Academic Press, San Diego 1990, pp. 151–251.
[20] R. Stosser, M. Nofz, Glastech. Ber. Glas. Sci. Technol. 67 (1994) 156–170.
[21] C.S. Sunandana, Bull. Mater. Sci. 21 (1998) 1–70.
[22] C.B. de Araújo, G. Boudebs, V. Briois, A. Pradel, Y. Messaddeq, M. Nalin, Opt. Commun. 260 (2006) 723–726.
[23] M. Nalin, G. Poirier, S.J.L. Ribeiro, Y. Messaddeq, E.J. Carvalho, L. Cescato, J. Non-Cryst. Solids 353 (2007) 1592–1597.
[24] E.L. Falcão-Filho, C.A.C. Bosco, G.S. Maciel, C.B. de Araujo, L.H. Acioli, M. Nalin, Y. Messaddeq, Appl. Phys. Lett. 83 (2004) 1292–1294.
[25] A.S. Gouveia-Neto, A.F. da Silva, L.A. Bueno, E.B. da Costa, J. Lumin. 132 (2012) 299–304.
[26] A. Jha, B. Richards, G. Jose, T. Teddy-Fernandez, P. Joshi, X. Jiang, J. Lousteau, Prog. Mater. Sci. 57 (2012) 1426–1491.
[27] L.A. Bueno, Vidros e vitrocerâmicas em sistemas oxifluoretosPhD Thesis UNESP — Araraquara, Brazil, 2003.
[28] M. Nalin, M. Poulain, Mi. Poulain, S.J.L. Ribeiro, Y. Messaddeq, J. Non-Cryst. Solids 284 (2001) 110.
[29] S. Stoll, A. Schweiger, J. Magn. Reson. 178 (2006) 42–55.
[30] J.M.F. Navarro, El Vidrio, 3rd Ed., Artegraf, Madri 1990, p. 448.
[31] J. Popplewell, L. Sakhnini, J. Magn. Magn. Mater. 149 (1995) 72–78.
[32] L.D. Bogomolova, N.A. Krasil'nikova, V.L. Bogdanov, V.D. Khalilev, V.V. Mitrofanov, J. Non-Cryst. Solids 188 (1995) 130–135.
[33] D. Möncke, E.I. Kamitsos, A. Herrmann, D. Ehrt, M. Friedrich, J. Non-Cryst. Solids 357 (2011) 2542–2551.
[34] P. Pascuta, M. Bosca, G. Borodi, E. Culea, J. Alloys Compd. 509 (2011) 4314–4319.
[35] I. Ardelean, M. Flora, J. Mater. Sci. 13 (2002) 357–362.
[36] S.P. Singh, R.P.S. Chakradhar, J.L. Rao, B. Karmakar, Physica B 405 (2010) 2157–2161.
[37] A. Mogus-Milankovic, L. Pavic, K. Srilatha, Ch.S. Rao, T. Srikumar, Y. Gandhi, N. Veeraiah, J. Appl. Phys. 111 (2012) 013714.
[38] I. Konidakis, Christos-Platon E. Varsamis, E.I. Kamitsos, D. Moncke, D. Ehrt, J. Phys. Chem. C 114 (2010) 9125–9138.
[39] D.L. Griscom, J. Non-Cryst. Solids 40 (1980) 211–272.
[40] J.S. Van Wieringen, Discuss. Faraday Soc. 19 (1955) 118–126.
[41] E. Simanek, K.A. Muller, J. Phys. Chem. Solids 31 (1970) 1027–1040.
[42] R.W.A. Franco, J.F. Lima, C.J. Magon, J.P. Donoso, Y. Messaddeq, J. Non-Cryst. Solids 352 (2006) 3414–3422.